INSTITUTE OF PHYSICS PUBLISHING and INTERNATIONAL ATOMIC ENERGY AGENCY NUCLEAR FUSION

Nucl. Fusion **44** (2004) S74–S82 PII: S0029-5515(04)79530-7

Transport modelling for ergodic configurations

A. Runov[1,a], S.V. Kasilov[2], N. McTaggart[1], R. Schneider[1], X. Bonnin[1], R. Zagórski[3] and D. Reiter[4]

[1] Max-Planck Institut für Plasmaphysik, EURATOM Association, D-17491 Greifswald, Germany
[2] Institute of Plasma Physics, National Science Center, 'Kharkov Institute of Physics and Technology', 310108 Kharkov, Ukraine
[3] Institute of Plasma Physics and Laser Microfusion, 00-908 Warsaw, Poland
[4] Institut für Plasmaphysik, Forschungszentrum Jülich GmbH EURATOM Association, Trilateral Euregio Cluster, D-52425 Jülich, Germany

E-mail: runov@ipp.mpg.de

Received 19 January 2004, accepted for publication 15 April 2004
Published 28 May 2004
Online at stacks.iop.org/NF/44/S74
doi:10.1088/0029-5515/44/6/S08

Abstract

The effect of ergodization, either by additional coils like in TEXTOR-dynamic ergodic divertor (DED) or by intrinsic plasma effects like in W7-X, defines the need for transport models that are able to describe the ergodic configuration properly. A prerequisite for this is the concept of local magnetic coordinates allowing a correct discretization with minimized numerical errors. For these coordinates the appropriate full metric tensor has to be known. To study the transport in complex edge geometries (in particular for W7-X) two possible methods are used.

First, a finite-difference discretization of the transport equations on a custom-tailored grid in local magnetic coordinates is used. This grid is generated by field-line tracing to guarantee an exact discretization of the dominant parallel transport (thus also minimizing the numerical diffusion problem). The perpendicular fluxes are then interpolated in a plane (a toroidal cut), where the interpolation problem for a quasi-isotropic system has to be solved by a constrained Delaunay triangulation (keeping the structural information for magnetic surfaces if they exist) and discretization. All toroidal terms are discretized by finite differences.

Second, a Monte Carlo transport model originally developed for the modelling of the DED configuration of TEXTOR is used. A generalization and extension of this model was necessary to be able to handle W7-X. The model solves the transport equations with Monte Carlo techniques making use of mappings of local magnetic coordinates. The application of this technique to W7-X in a limiter-like configuration is presented. The decreasing dominance of parallel transport with respect to radial transport for electron heat, ion heat and particle transport results in increasingly steep profiles for the respective quantities within the islands.

PACS numbers: 52.55.Dy, 52.55.Rk

1. Introduction

This paper is a review of our work done on three-dimensional fluid modelling in ergodic magnetic fields using the multiple coordinate systems approach according to [1–6]. To be able to deal with very general magnetic configurations, one needs a correspondingly general numerical tool. The model presented here is based on local magnetic coordinate systems (LMCSs) and couples neighbouring systems with high accuracy. The method has a large variety of applications, mainly in the stellarator community, but also for tokamaks (e.g. TEXTOR-dynamic ergodic divertor (DED), DIII-D).

This work was inspired by the idea of the TEXTOR-DED [7]. Here, one installs a special set of magnetic coils to obtain additional control over the fluxes in the plasma periphery. Indeed, the stronger the magnetic perturbation, the larger the islands on the resonant surfaces, which eventually overlap and build a so-called 'ergodic layer': the behaviour of a field line becomes stochastic (two originally neighbouring field lines diverge from each other exponentially with a Kolmogorov characteristic length L_K), and we obtain a non-zero projection of the strong parallel heat transport onto the radial direction

[a] Author to whom any correspondence should be addressed.

and, therefore, a flattening of the temperature profile—see the well-known expression from Rechester and Rosenbluth [8] for the amplification of the radial diffusion because of this mechanism:

$$\chi_r^{(\mathrm{RR})} = D_{\mathrm{fl}} D_{\|e} \left[L_K \ln \left(\frac{1}{r k_\theta} \left(\frac{\chi_{\|e}}{\chi_\perp} \right)^{1/2} \right) \right]^{-1}, \qquad (1)$$

where D_{fl} is the field line diffusion coefficient, $k_\theta = m/r$ the characteristic perpendicular wave number, L_K the Kolmogorov length, r the minor radius and m is the poloidal number of the perturbation; $\chi_\|^e$, $\chi_\perp^e$ are the 'intrinsic' transport coefficients arising from the underlying plasma transport. The advantage of such an ergodic layer lies in the possibility of improving the conditions for radiation from this region by flattening the radial temperature profile at some optimal level.

Configurations of this kind are very general: they contain intact magnetic surfaces, islands, ergodic and open field lines, and are, in that respect, similar to the edge region of stellarators. The main problem for transport modelling in such mixed regions is as follows: the coordinate system must be aligned to the unstructured magnetic field. Indeed, let us consider a constant magnetic field in a Cartesian coordinate system aligned with the field lines. The diffusion tensor here has a desirable diagonal form, whereas in the case of a misaligned coordinate system we have non-zero elements everywhere. If we try to solve our equation in this misaligned coordinate system numerically, we will have an artificial perpendicular heat flux proportional to the parallel diffusion coefficient, leading to the so-called 'numerical diffusion'. For realistic plasma edge conditions, the ratio between $\chi_\|$ and $\chi_\perp$ can be up to eight orders of magnitude, and the numerical diffusion becomes a severe problem. The difficulty is obviously common to all numerical methods, and in practice we are forced to use the magnetic field line itself as one of the local coordinate axes.

2. Basic problem

Formally, in fluid dynamics we deal with a convection–conduction differential equation for some generalized 'fluid quantity' f in vector form

$$\frac{\partial f}{\partial t} - \nabla \cdot [D_\perp \nabla f + (D_\| - D_\perp) \boldsymbol{h}\boldsymbol{h} \cdot \nabla f - (\boldsymbol{V}_\perp + \boldsymbol{h} V_\|) f] = S - \nu f. \qquad (2)$$

Here, $\boldsymbol{h} = \boldsymbol{B}/B$ is a unit vector along the magnetic field, $D_\perp$, $D_\|$, $\boldsymbol{V}_\perp$ and $V_\|$ are the anomalous (usually constant) perpendicular and classical parallel generalized diffusion coefficients, and perpendicular and parallel convection velocities, respectively. In general curvilinear coordinates x^i, equation (2) can be written in the following form:

$$\frac{\partial f}{\partial t} - \frac{1}{\sqrt{g}} \frac{\partial}{\partial x^i} \sqrt{g} \left(D^{ij} \frac{\partial f}{\partial x^j} - V^i f \right) = S - \nu f, \qquad (3)$$

where $D^{ij} = D_\perp^{ij} + D_\|^{ij}$ and $V^i = V_\perp^i + V_\|^i$ are diffusion tensors and velocities appropriate for f,

$$D_\perp^{ij} = D_\perp (g^{ij} - h^i h^j), \qquad D_\|^{ij} = D_\| h^i h^j,$$
$$V_\perp^i = \boldsymbol{V}_\perp \cdot \nabla x^i, \qquad V_\|^i = V_\| h^i. \qquad (4)$$

Here, g, $g^{ij} = (\nabla x^i) \cdot (\nabla x^j)$ and $h^i = \boldsymbol{h} \cdot \nabla x^i$ are the determinant and contravariant components of the metric tensor, and of the unit vector along the magnetic field, respectively. If we choose a coordinate system in which the magnetic field has only one non-zero component, we guarantee the separation of the parallel and perpendicular fluxes (i.e. if $h^1 = h^2 = 0$, we have a contribution from $D_\|$ in D^{33} only).

The question now is how to build such a coordinate system. We begin by choosing a surface (called the reference cut) which intersects all field lines of interest and draw some reasonable (e.g. Cartesian) mesh on this cut. We now trace field lines through the mesh lines. The surfaces we obtain are our coordinate surfaces. It should be noted that a similar procedure is used for building Clebsch stream functions (see, e.g. [9]). The metric of this system can be obtained by field line tracing: indeed, the real space coordinates are linked with these magnetic coordinates by field line tracing, and we can extend this procedure to calculate the relevant transformation matrix (see [4, 6]). These coordinates can be used locally. By this, we mean that more than one reference cut (and, therefore, multiple coordinate systems) can be used, in order to keep the scope of a single system well below the Kolmogorov length. The price for simplicity of the representation of the magnetic field in these cordinates is clear: the system is non-periodic, i.e. the coordinate surfaces of neighbouring systems overlap arbitrarily at the interface between the two systems.

If we try to solve the problem by interpolation, we induce numerical diffusion of the same nature as before: an artificial contribution of the parallel flux to the radial transport. For instance, if one were to pass a beam (a δ-function) through such a system, one would obtain a response in all four corners of the cell on the interface between two neighbouring coordinate systems, and then on the next interface it would spread further. There are two proposed methods for dealing with this phenomenon.

The first is to optimize the mesh on the reference cut, i.e. to produce it by field line tracing itself. Indeed, if we could build a mesh consisting of footprints of field lines only, we would solve the problem. This idea is good for the field lines starting and ending on the wall, or for closed field lines. Any other field line can be treated as 'almost closed' as long as the following criterion of the negligibility of the numerical diffusion is fulfilled: $\Delta \ll L_\| \sqrt{\chi_\perp / \chi_\|}$, where Δ is the excursion between the start and end points as measured on the cut and $L_\| \approx 2\pi R N$ is the distance between the same points measured along the field line with $N \approx 100$ toroidal turns. We select only those field lines which come within $\Delta = 1$ mm of closing upon themselves and close them artificially. Only such field lines are involved in building the mesh. This minimizes the induced numerical diffusion to about $10^{-4}\,\mathrm{m^2\,s^{-1}}$. The penalty one pays for this method is an unstructured mesh.

The second idea is to switch to a Monte Carlo method with an appropriate mapping technique, such as the one described below. In this case, the problem becomes one of passing a particle from one coordinate system to another, much like the baton in a relay race, instead of mesh re-interpolation.

3. Finite-difference ansatz

The basic set-up for the numerical realization of the first approach [4] is as follows: we choose 20 reference cuts per

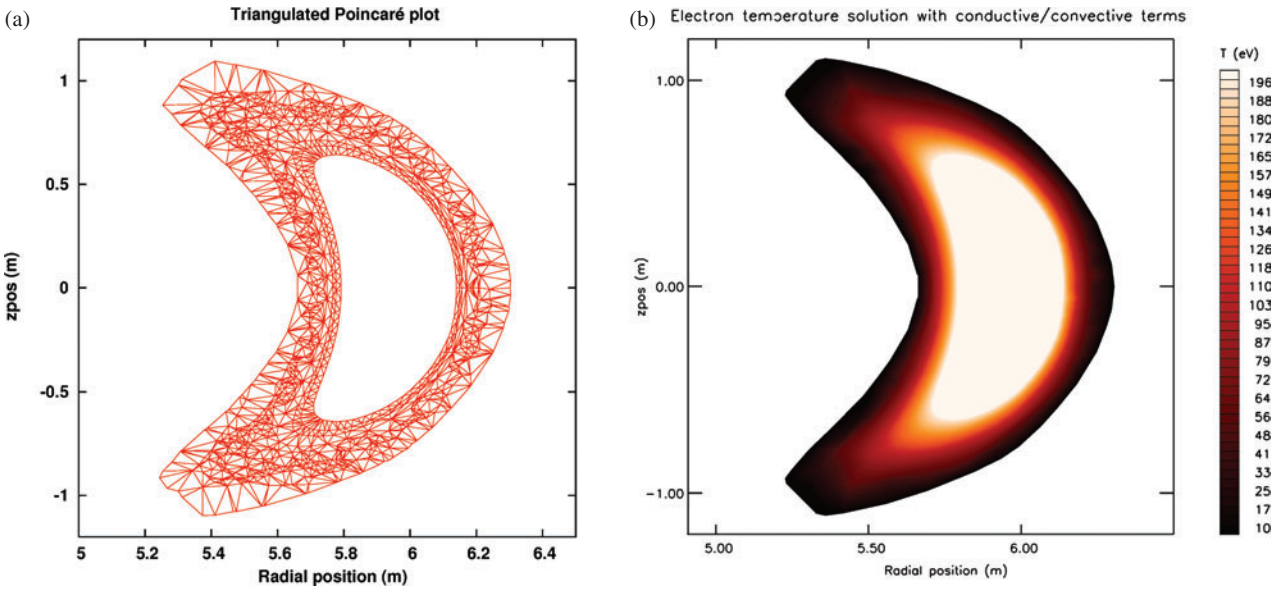

Figure 1. (*a*) Triangulated Poincaré plot for the W7-X configuration; (*b*) corresponding temperature profile.

toroidal turn and build the unstructured mesh using 'almost closed' field lines or lines hitting the wall, and discretize our equations with a finite-difference scheme.

The next question to answer is about how local a single coordinate system can be. One must be able to write and discretize the divergence of gradients within its scope. In other words, it must contain the whole stencil we use for the discretization. Thus, our local coordinate system is a moving patch centred on the point of interest and covering three neighbouring reference cuts simultaneously. The advantage of this system is obvious: if we switch the perpendicular diffusion off, we will use only the three points in our scheme located along the same field line, at its intersections with the reference cuts. It means that we achieve the desirable separation between parallel and perpendicular transport in the scheme.

The rest is more or less conventional work with an unstructured mesh: the perpendicular problem is isotropic, and the choice of the numerical method is uncritical. We build the mesh with the help of a modification of Delaunay triangulation—a method commonly used in finite elements calculations (see figure 1(*a*)). The corresponding electron temperature profile is presented in figure 1(*b*).

4. Monte Carlo method

In this approach we model a diffusion-like equation using the random walk of Brownian particles. It is important to stress here the difference from kinetic Monte Carlo modelling used in the low collisionality regime: in that case the fastest time scale corresponds to the regular test particle drift motion described by ordinary differential equations with smooth coefficients, while stochastic changes of particle velocity which model slow collisional diffusion in velocity space are small and can be treated as a perturbation in the lowest order. Therefore, high-order integrators are useful for that problem. However, in the case of diffusion-dominated transport, high-order integration is a nontrivial numerical problem (see, e.g. this book [10]). For example, let us consider a one-dimensional Fokker–Planck equation

$$\frac{\partial f}{\partial t} = \frac{\partial^2}{\partial x^2} Df - \frac{\partial}{\partial x} V_c f$$

and the equivalent Ito stochastic differential equation

$$\mathrm{d}x = V_c \,\mathrm{d}t + \sqrt{2D}\,\mathrm{d}W(t),$$

where W is a so-called Wiener process. The simplest method to sample stochastic trajectories is the first-order integrator similar to the Eulerian scheme for ODEs: all differential operators are replaced by differences:

$$\Delta x = V_c \Delta t + \sqrt{2D\Delta t}\,\xi, \qquad \text{where } \langle \xi \rangle = 0, \quad \langle \xi^2 \rangle = 1. \tag{5}$$

The second-order integrator is already much more complex (see, e.g. [11]):

$$\begin{aligned}\Delta x = {} & V_c \Delta t + \sqrt{2D\Delta t}\,\xi + \sqrt{D}\frac{\partial \sqrt{D}}{\partial x}\Delta t(\xi^2 - 1) \\ & + \left(V_c \frac{\partial \sqrt{D}}{\partial x} + \sqrt{D}\frac{\partial V_c}{\partial x} + D\frac{\partial^2 \sqrt{D}}{\partial x^2} \right) \frac{\Delta t^{3/2}}{\sqrt{2}}\xi \\ & + \left(V_c \frac{\partial V_c}{\partial x} + D\frac{\partial^2 V_c}{\partial x^2} \right) \frac{\Delta t^2}{2}.\end{aligned} \tag{6}$$

One can see that the number of terms we need grows with the order of the scheme much faster than for ordinary differential equations. In the three-dimensional case, the number of terms for such schemes becomes so large that the calculation effort becomes unacceptable. Furthermore, in our nonlinear case, the transport coefficients D and V_c are sampled numerically as well. Therefore, they are noisy, and calculation of their higher order derivatives is undesirable. Hence, we are forced to restrict ourselves to the simplest first-order (so-called Euler–Maruyama) integrator. A special set of optimized local magnetic coordinates discussed in section 6 allows us to keep both time-step and numerical errors acceptable for such a

scheme: in these coordinates, the main limitation of the time step which comes from the fastest parallel transport timescale is relaxed by making corresponding transport coefficients slowly varying along the field lines. (A much stronger limitation of the time step due to the parallel transport, which must accurately follow the field lines, does not appear in our magnetic coordinates.)

The outline of the algorithm is as follows: we rewrite the convection–conduction equation (3) in a Fokker–Planck form:

$$\frac{\partial N}{\partial t} - \frac{\partial}{\partial x^i}\left(\frac{\partial}{\partial x^j} D^{ij} N - V_c^i N\right) = \sqrt{g} S - \nu N, \quad (7)$$

where $N = \sqrt{g} f$ and

$$V_c^i = V^i + \frac{1}{\sqrt{g}} \frac{\partial}{\partial x^j} \sqrt{g} D^{ij}, \quad (8)$$

choose some appropriate initial profile and fill the computation domain with test particles distributed in accordance with this profile. On a time step, every particle gets a kick (random for diffusion and regular for convection), and the distribution evolves. The algorithm can be understood in terms of Green's functions: if a lot of particles are started at the same point and counted after a time interval Δt, their distribution gives a statistical approximation to the equation response to a δ-function. Therefore, taking starting points distributed in accordance with the initial profile, the convolution integral of this response function with the initial distribution is sampled. This integral is the desired solution.

The conditional sink, νf, and source, S, terms in (3) are modelled during a single time step Δt by terminating test particle orbits with probability $\nu \Delta t \ll 1$ and adding new particles with the distribution $S \Delta t$, respectively.

It should be noted that two different time steps are used here. The first one, Δt, is the time for a single particle jump (entering equation (5)), which is defined by the gradients of plasma parameters (see also section 6) or by the distance to the wall. The second one, Δt_r, is the actualization time of transport coefficients: since transport coefficients are nonlinear functions of plasma parameters, they are adjusted after time intervals $\Delta t_r \ll \tau_r$, where τ_r is a typical profile relaxation time. Within Δt_r plasma parameters are kept constant, and time averaging is performed. The magnitude of this time interval is strongly problem dependent: if we are interested in a true time evolution, it has to be comparable with Δt. In the limiting case of a linear problem (with fixed transport coefficients) it can be made very large. As long as we are looking for a steady-state solution, Δt_r should be small enough to provide the convergence for our iterations (normally, we use a fraction of the radial relaxation time).

5. Interpolated cell mapping

As mentioned before, a particular LMCS is used within its own domain. For example, for stellarator modelling such a domain is normally the toroidal magnetic field period. Whenever a test particle travels to the neighbouring LMCS, we have to perform a transformation of the pair of 'perpendicular' coordinates (which label field lines in a given LMCS) with high accuracy to avoid artificial cross-field transport induced by fast parallel transport. These two coordinates are actually the coordinates on the LMCS reference cut plane of its intersection (or footprint) with the field line passing through the point of interest. Thus, the new coordinates are the coordinates of the same field line's intersection point but with the reference cut plane of the neighbouring LMCS. The problem is solved by means of an interpolated cell mapping procedure [1, 12, 13]. The main idea here is to trace field lines starting in the knots of the two-dimensional mesh on the reference cut of the old LMCS (e.g. with the GOURDON code) and use interpolation for the points in between. In other words, real space coordinates of the field line footprint on the reference cut of a new LMCS are treated as two two-dimensional functions of its starting coordinates on the old LMCS reference cut. These functions are given by interpolation of pre-computed data. The accuracy needed depends on the ratio between the parallel and perpendicular transport. The estimations show that bicubic spline interpolation provides enough accuracy for acceptable mesh sizes (see appendix A in [1]).

For stellarator applications coordinates have been optimized in order to make the SOL region in these coordinates close to a rectangle with one of the sides being the boundary with the core plasma. Indeed, the reference cut mesh does not have to be Cartesian—it is more natural to choose as coordinate lines a family of curves given by a linear interpolation between the cross section of the last closed magnetic surface on the reference cut and some curve which smoothly envelops the cross section of the wall. In [4], this last curve was represented by another magnetic surface outside the island region. The variational moments equilibrium code (VMEC) angle-like variable u could be chosen as the second family of curves (as shown in figure 2(a)). The transformation between Cartesian coordinates and this new mesh is given in the form of a Fourier expansion over VMEC angles. The inverse transformation and the calculation of the metric tensor of this system is only possible numerically (see [4]).

The results in non-ergodic regions are very good: the Poincaré plots obtained with mapping and field line tracing are optically identical as one can see from the overlay of field line tracing and mapping on figure 2(b). After 600 field periods, one gets a deviation of only 8×10^{-3} cm (to be compared with the thickness of the SOL being several centimetre).

In ergodic regions, the exponential divergence of the magnetic field lines amplifies both the numerical and physical perpendicular diffusions and the estimation presented in appendix A of [1] remains valid.

6. Optimized coordinates

The restriction on the time step in Monte Carlo is clear: a single particle step must be small compared to the gradient length of the diffusion coefficient. In equation (7), non-zero components of the parallel diffusion tensor and effective convection velocity depend on both plasma and magnetic field parameters:

$$D_\parallel^{33} = D_\parallel (h^3)^2, \qquad V_{\parallel c}^3 = V_\parallel h^3 + \frac{1}{\sqrt{g}} \frac{\partial}{\partial x^3} \sqrt{g} D_\parallel^{33}. \quad (9)$$

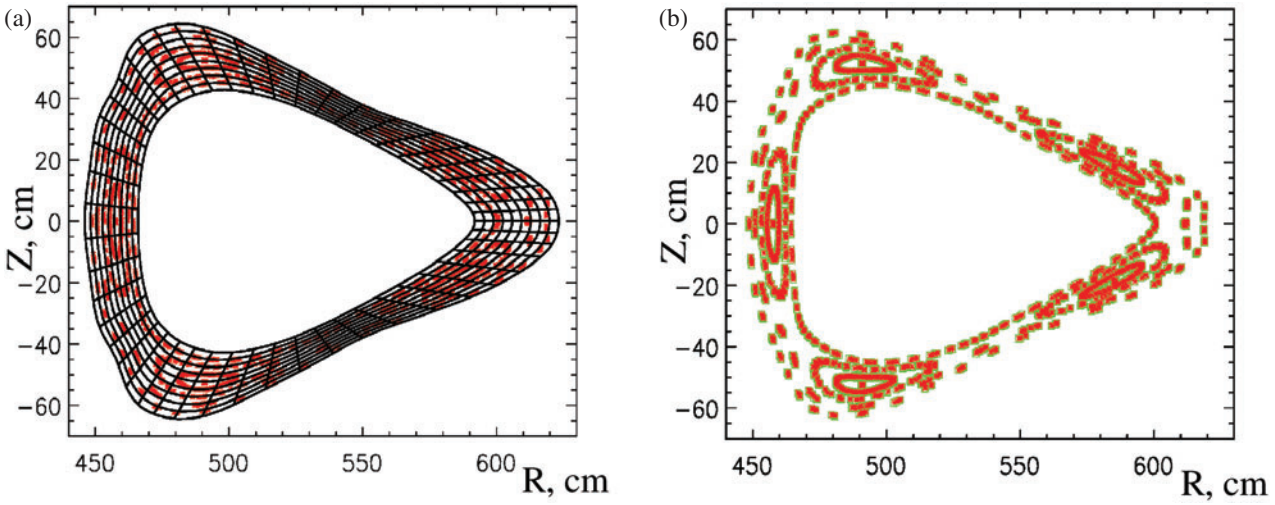

Figure 2. (*a*) Mesh on the reference cut optimized for W7-X; (*b*) overlap of mapping and field-line tracing for this mesh [4].

The plasma parameter dependence comes through the non-linear parallel diffusion coefficient, $D_\parallel$, whereas the magnetic field dependence comes through h^3 and the metric determinant. In the case of the heat conductivity equation, the problem arises near the inner boundary of the domain: here a high constant temperature results in a very large parallel heat diffusion, while the characteristic length of the magnetic field is one period or even the distance between the coils. This means that reproducing this constant numerically will be very CPU intensive. To allow for long parallel steps, magnetic field dependences must be eliminated. This is done in two steps.

As a first step, assuming toroidal reference cuts, $\varphi = \text{const}$, we define the third, 'parallel', coordinate as follows:

$$x^3 = S_{(m)} \int_{\varphi_{\min}^{(m)}}^{\varphi} \mathrm{d}\varphi' \frac{(B)^2}{B^\varphi} + \varphi_{\min}^{(m)}. \tag{10}$$

Here, the integration over the toroidal angle φ is performed along the magnetic field line, $x^1 = \text{const}$, $x^2 = \text{const}$, B is the magnetic field modulus, B^φ the contra-variant toroidal component of the magnetic field and $\varphi_{\min}^{(m)}$ is the lower boundary of the domain of the mth LMCS. The scaling factor which keeps the new coordinate in the fixed range $[\varphi_{\min}^{(m)}, \varphi_{\max}^{(m)}]$ is

$$S_{(m)} = (\varphi_{\max}^{(m)} - \varphi_{\min}^{(m)}) \left(\int_{\varphi_{\min}^{(m)}}^{\varphi_{\max}^{(m)}} \mathrm{d}\varphi' \frac{(B)^2}{B^\varphi} \right)^{-1}, \tag{11}$$

where $\varphi_{\max}^{(m)}$ is the upper boundary of the domain of the mth LMCS. As follows from (10), the 'parallel' component of the magnetic field, $B^3 = \partial(x^1, x^2, x^3)/\partial(x^1, x^2, \varphi) B^\varphi$, scales as the square of the magnetic field modulus $(B)^2$ along the magnetic field lines. In addition, due to Gauss' law,

$$\operatorname{div} \boldsymbol{B} = \frac{1}{\sqrt{g}} \frac{\partial}{\partial x^3} \sqrt{g} B^3 = 0,$$

the Jacobian scaling along the field lines is $\sqrt{g} \sim (B)^{-2}$. Therefore, the combination $(h^3)^2 \sqrt{g}$ is constant on the field line and, as a result, its derivative in the convection velocity V_c^3 is zero.

As a second step, the coefficient D^{33} itself should be made 'almost constant' (it would be an exact constant for constant temperature). This is achieved by re-definition in equation (7) of the unknown f and of the transport coefficients D^{ij} and V_c^i:

$$f = \mu \tilde{f}, \qquad \tilde{D}^{ij} = \mu D^{ij}, \qquad \tilde{V}_c^i = \mu V_c^i, \tag{12}$$

where $\mu(\boldsymbol{r})$ is some scalar function of the coordinates. Let us introduce a particular form of the scaling factor μ, which will serve two purposes:

- The new parallel diffusion tensor component, $\tilde{D}_\parallel^{33}$, and the derivative term in the new parallel effective convection velocity component, $\tilde{V}_{\parallel c}^3$, will be dependent on x^3 only through a dependence on plasma parameters, but not through the geometrical terms, namely, $\sqrt{g}$ and h^3. This removes the limitation on the parallel step by the scaling of the magnetic field in this direction.
- The parallel effective convection velocity will not contain density derivatives, thus reducing the influence of statistical noise in this quantity on the Monte Carlo process.

Both these conditions are satisfied by

$$\mu = \frac{c_0 n_e}{(B)^2}, \tag{13}$$

where c_0 is some constant which we are free to choose (see [6]). The resulting efficiency of the code is improved by about two orders of magnitude.

7. Basic transport equations of E3D

The code E3D (ergodicity in three dimensions) combines all the ideas mentioned above. The physics model used in the code is the usual set of Braginskii equations. They are all of the convection–conduction form and, therefore, can be solved by means of the multiple coordinate systems approach.

The continuity equation is presented in its standard form ($n_i = n_e \equiv n$):

$$\frac{\partial n}{\partial t} + \nabla \cdot (\boldsymbol{h} V_\parallel n + \boldsymbol{V}_\perp n) = S_n - \nu_n n, \tag{14}$$

where

$$\boldsymbol{V}_\perp \equiv \frac{D_\perp}{n}(\boldsymbol{h}\,\boldsymbol{h}\cdot\nabla n - \nabla n).$$

It is convenient to work with total parallel momentum, and the sum of the ion and electron momentum equations is rewritten in this form ($\boldsymbol{V}_i = \boldsymbol{V}_e \equiv \boldsymbol{V}$; $p_\parallel \equiv mn\boldsymbol{h}\cdot\boldsymbol{V}$):

$$\frac{\partial p_\parallel}{\partial t} + \nabla\cdot((\boldsymbol{V}_{\perp V} + \boldsymbol{h}V_{\parallel V})p_\parallel - D_{\perp V}\nabla p_\parallel - (D_{\parallel V} - D_{\perp V})\boldsymbol{h}\boldsymbol{h}\cdot\nabla p_\parallel) = S_V - \nu_V p_\parallel. \tag{15}$$

Here,

$$\boldsymbol{V}_{\perp V} \equiv \left(1 - \frac{\eta_A}{mnD_\perp}\right)\boldsymbol{V}_\perp, \qquad V_{\parallel V} \equiv V_\parallel + \frac{4\eta_0}{3mn^2}\boldsymbol{h}\cdot\nabla n,$$

$$D_{\perp V} \equiv \frac{\eta_A}{mn}, \qquad D_{\parallel V} \equiv \frac{4\eta_0}{3mn}, \qquad \boldsymbol{N} \equiv \boldsymbol{h}\cdot\nabla\boldsymbol{h},$$

$$\nu_V \equiv -\boldsymbol{V}_\perp\cdot\boldsymbol{N} + \frac{\eta_0}{mn}(\operatorname{div}\boldsymbol{h})^2 + \frac{2}{3mn}\boldsymbol{h}\cdot\nabla\eta_0\operatorname{div}\boldsymbol{h},$$

$$S_V \equiv -\boldsymbol{h}\cdot\nabla p + \boldsymbol{h}\cdot\boldsymbol{F}_S + mn\boldsymbol{V}_\perp\cdot(\boldsymbol{V}_\perp\cdot\nabla)\boldsymbol{h} - \left(\frac{2}{3}\boldsymbol{h}\cdot\nabla + \operatorname{div}\boldsymbol{h}\right)\eta_0(3\boldsymbol{V}_\perp\cdot\boldsymbol{N} + \operatorname{div}\boldsymbol{V}_\perp),$$

where $p = n(T_i + T_e)$ is the plasma pressure, $\boldsymbol{F}_S$ an external force density and η_0 and η_A are classical parallel and anomalous shear viscosity coefficients, respectively. All the source terms here are of a purely geometrical nature: imagine a particle, representing a 'piece of parallel momentum' jumping across the magnetic field, the momentum it carries is no longer parallel to the local field line. These terms account for this effect.

Heat conductivity equations for species $\alpha = e, i$ are rewritten for the unknown internal energy:

$$\frac{\partial u_\alpha}{\partial t} + \nabla\cdot((\boldsymbol{V}_{\perp\alpha} + \boldsymbol{h}V_{\parallel\alpha})u_\alpha - D_{\perp\alpha}\nabla u_\alpha - (D_{\parallel\alpha} - D_{\perp\alpha})\boldsymbol{h}\boldsymbol{h}\cdot\nabla u_\alpha) = S_\alpha - \nu_\alpha u_\alpha. \tag{16}$$

Here,

$$u_\alpha \equiv \frac{3}{2}nT_\alpha, \qquad \boldsymbol{V}_{\perp\alpha} \equiv \left(1 - \frac{D_{\perp\alpha}}{D_\perp}\right)\boldsymbol{V}_\perp,$$

$$V_{\parallel\alpha} \equiv V_\parallel + \frac{1}{n}D_{\parallel\alpha}\boldsymbol{h}\cdot\nabla n, \quad D_{\perp\alpha} \equiv \frac{2\kappa_{\perp\alpha}}{3n}, \quad D_{\parallel\alpha} \equiv \frac{2\kappa_{\parallel\alpha}}{3n},$$

$\kappa_{\perp\alpha}$ and $\kappa_{\parallel\alpha}$ are anomalous perpendicular and classical parallel heat conductivity coefficients.

The three equations (14)–(16) are implemented in E3D completely, and the parallel momentum equation (15) is implemented in a test (one-dimensional) geometry only. The additional geometrical terms will be included later.

Complex codes require extensive benchmarking as a systematic method to eliminate mistakes. Cross-benchmarking between different codes is the most suitable approach. The electron heat conductivity equation in a single island geometry has been tested. After several simplifications, the problem has been reduced to a linear two-dimensional problem and solved with E3D, BoRiS (which is a three-dimensional finite volume code) and pre-packaged subroutines from the NAG library. Very good agreement for all three codes has been demonstrated [2].

8. TEXTOR-DED

In TEXTOR-DED one installs a special set of coils to obtain additional control over the fluxes in the plasma periphery. The achievement of a well-developed ergodicity in this configuration seems problematic, since in reality one obtains a very complex mixture of island remainders, ergodic and laminar field lines. This provides some contribution from the parallel heat flux into radial transport and, therefore, a flattening of the temperature profile. The price is clear: the heat flux on the limiter concentrates in several stripes produced by 'fingers'—regions where the field lines starting on the wall enter the ergodic field region (there can be four to eight stripes depending on the plasma current; see figure 14 in [5]). One can also see the calculated electron temperature distribution for a typical case from TEXTOR-DED, in figure 13 in [5]. As expected, it reflects the structure of the magnetic field. This leads to the idea of smearing out the 'hot stripes' by means of dynamical sweeping. A dynamical operation mode using an ac power supply for the perturbation coils will change the magnetic field pattern and by this the electron temperature distribution. The dynamical operation and its time-varying electron temperature distribution results in time-varying limiter power loads. This method is planned for TEXTOR (hence the name *dynamic* ergodic divertor) with a wide range of frequencies (from 50 Hz to 10 kHz). E3D in its present form is able to work in a quasi-static approximation only (this means that the re-building of plasma profiles is faster than the variation of the magnetic field; this is valid up to about 100 Hz). In this case, one can treat the dynamic situation as a sequence of steady-state solutions. The time-averaged effect, even in the lowest frequency limit, is clear: the peak power load is reduced by almost one order of magnitude even in the low-frequency limit of 50 Hz (cf figures 14 and 15 of [5]).

In these realistic cases, the field is only partially ergodic. In this work [1] we asked a somewhat academic question: how well does the classical Rechester–Rosenbluth formula (1) describe the situation? Formally, one can calculate the 'effective heat conductivity' by dividing the calculated heat flux by the temperature gradient (using the angle-averaged values). It should be noted that only the parallel component of the total radial heat flux is needed for this comparison. The results for linear (without the temperature dependence of the parallel heat conduction) and nonlinear (taking account of this dependence) cases are presented in figure 3. One can see that the RR formula provides the correct order of magnitude estimate up to (but not including) the 'laminar zone', i.e. in the region without direct contact with the wall. In the neighbouring (laminar) region, another mechanism dominates: not the 'braiding' of field lines, but the direct contact of the field lines with the wall.

9. Effect of noise-like static magnetic field perturbations on the radial electron heat conductivity

The existence of internal transport barriers (ITBs) is one of the important features of anomalous transport, which is under investigation in present-day tokamak experiments. ITBs have been observed in experiments with reversed shear profiles.

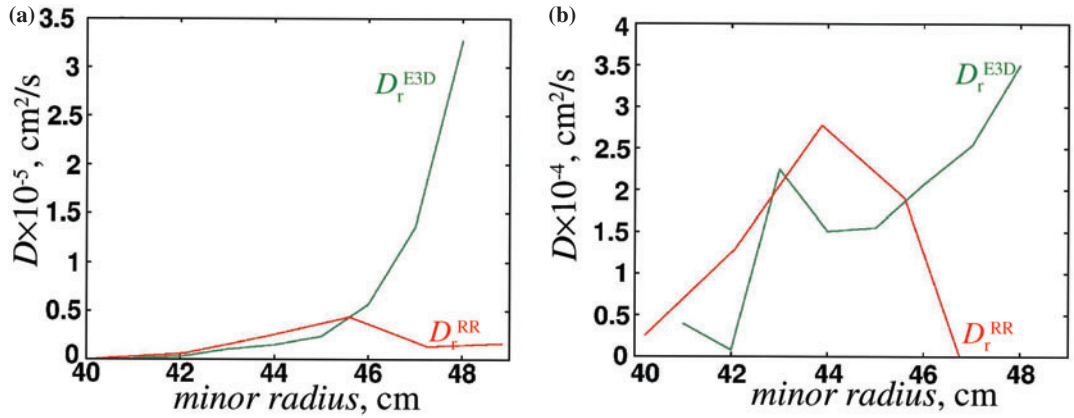

Figure 3. Comparison of effective diffusion coefficient (green) and Rechester–Rosenbluth prediction (red) versus minor radius (*a*—linear case, *b*—nonlinear case) [1].

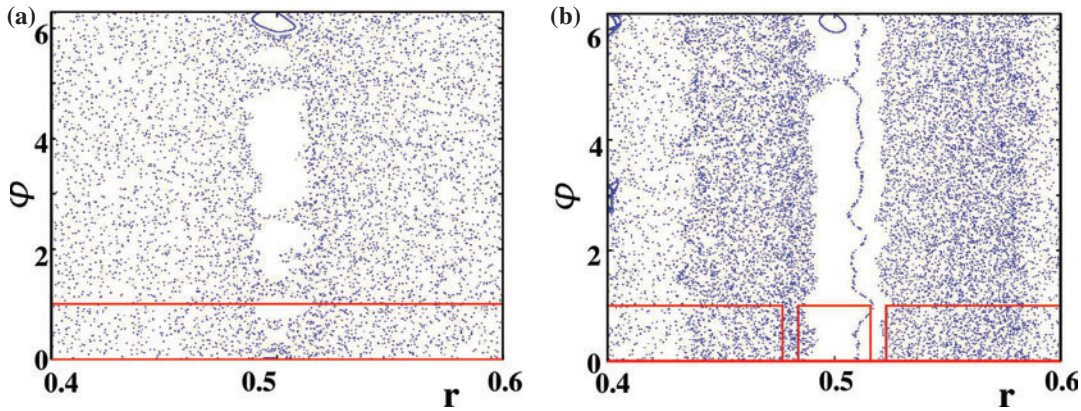

Figure 4. Poincaré plots for different amplitudes of perturbation: (*a*) $\varepsilon = 2.6666 \times 10^{-4}$; (*b*) $\varepsilon = 1.3333 \times 10^{-4}$ (overlapping criterion violated) [3].

A particular case is the RTP tokamak, where electron ITBs have been observed around low-order rational magnetic surfaces in the case of a monotonic safety factor profile [14]. In [3], the possibility of electron ITBs in the presence of additional radial transport due to static randomly phased magnetic field perturbations with a broad spatial spectrum has been investigated. For this, a model geometry consisting of a straight periodic cylinder with a rotational transform angle, $\iota = \iota(r) = 1/q(r)$, monotonically changing with radius has been assumed. The perturbing magnetic field was noise-like,

$$B_r = \sum_{m,n=-\infty}^{\infty} b_{m,n} \cos(m\theta - n\varphi + \alpha_{m,n}), \qquad (17)$$

where θ, $\varphi = z/R$ and $2\pi R$ are poloidal and the toroidal angles, and the cylinder period, respectively. Here, Fourier harmonics are randomly phased with respect to each other with phases $\alpha_{n,m}$. For the modelling, the following spectrum for the magnetic field perturbation has been used,

$$b_{m,n} = \varepsilon\,(m/\bar{m})^{\gamma}\,\Theta\,(|m| - \bar{m})\,\Theta\,(|n| - \bar{n})\,, \qquad (18)$$

where ε denotes the amplitude of the perturbation. Here, $\bar{m} \gg 1, \bar{n} \gg 1$ are poloidal and toroidal widths of the spectrum, respectively, and Θ is the Heavyside step function. Such a broad spectrum represents short scale turbulent perturbations of the magnetic field, which have their spectral maximum located in the region of large perpendicular wavenumbers.

If the perturbation amplitude is large enough, the magnetic field becomes ergodic over the whole radius due to the overlapping of the islands formed by various harmonics at different resonant surfaces with $\iota(r) = n/m$. As a consequence of parallel heat transport along such braided magnetic field lines, the 'anomalous' heat conductivity appears.

If the perturbation amplitude is moderate, regions where intact KAM surfaces exist or, at least, the diffusion of field lines is reduced, appear around low-order rational magnetic surfaces (see figure 4 where the Poincaré plots for two different values of the perturbation amplitude ε are shown). This is due to the fact that the spacing between radial positions of resonances from the limited range of wavenumbers, $|m| \leqslant \bar{m}$, $|n| \leqslant \bar{n}$, is not homogeneous and is much larger than average if one of the neighbouring resonances is a low-order resonance. The criterion for the formation of such a region around a low-order resonant radius with $\iota(r) = n_0/m_0$ is

$$\varepsilon R(m_0\bar{m})^{3/2} \left|\frac{\mathrm{d}\iota(r)}{\mathrm{d}r}\right| \log^{1/2}\left(\frac{\bar{m}}{m_0}\right) < 1. \qquad (19)$$

Such a criterion is valid for $\gamma > \frac{1}{2}$. Taking $\gamma = 1$, the E3D code has been used to calculate radial temperature profiles

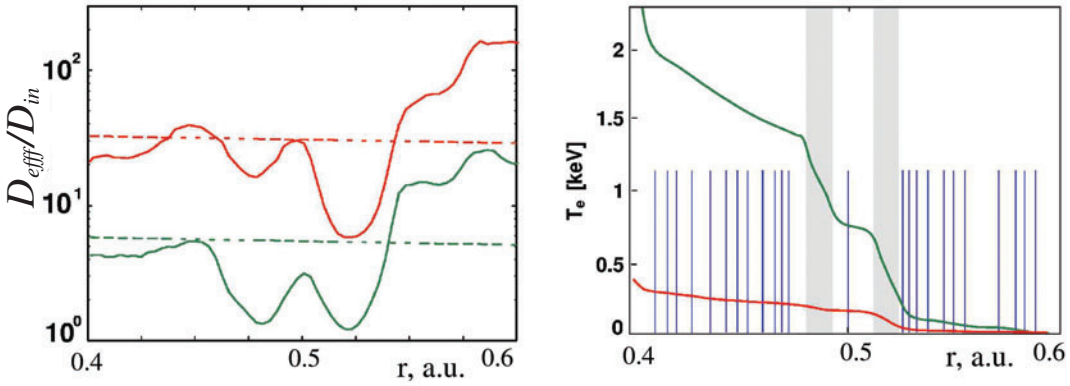

Figure 5. (*a*) Ratio between effective diffusion calculated with E3D and intrinsinc value; (*b*) temperature profiles (red—$\varepsilon = 2.6666 \times 10^{-4}$, green—$\varepsilon = 1.3333 \times 10^{-4}$) [3].

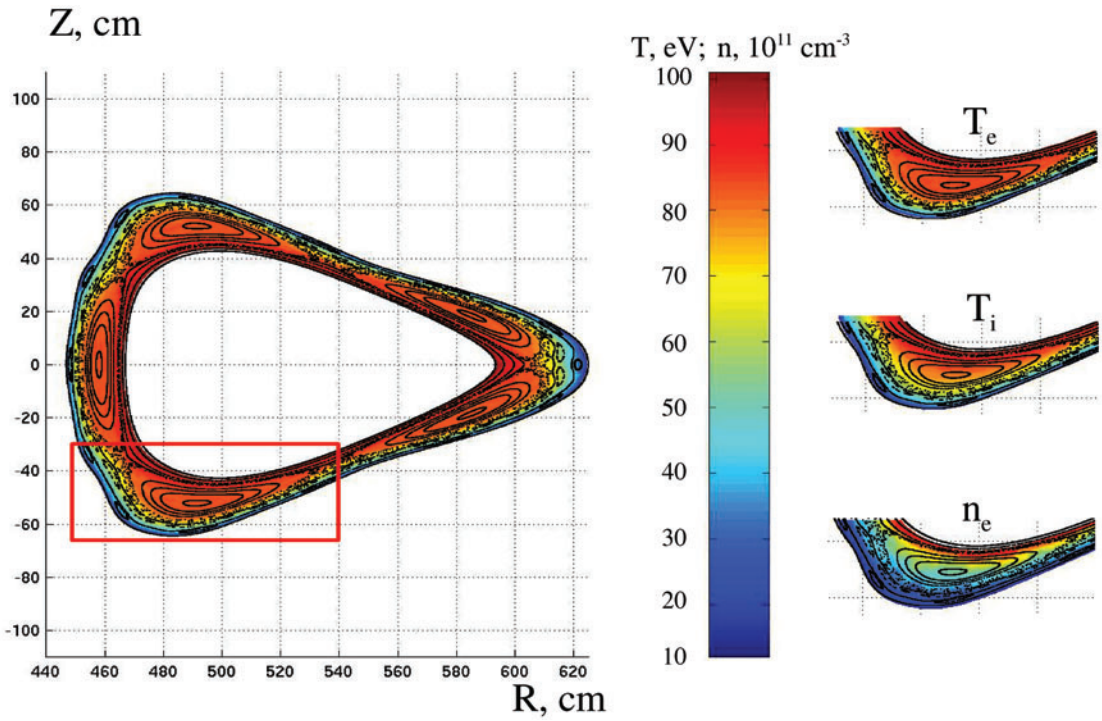

Figure 6. Results for W7-X geometry: electron and ion temperatures, plasma density [6].

for the two cases shown in figure 4 and to evaluate from these profiles the effective radial heat diffusion coefficient. If the perturbation is small enough, the effective heat diffusion drops to its intrinsic value and a barrier-like temperature profile develops around the low-order rational ι point ($\iota = \frac{1}{2}$, see figure 5). This mechanism is, therefore, a candidate for the creation of ITBs.

10. W7-X

In this section, we present results for the W7-X magnetic geometry (without real divertor plates, an artificial boundary being set on the outer closed magnetic surface instead, [6]). We prescribe 10 eV for both temperatures and 10^{12} cm^{-3} for the density at the outer edge of the plasma. On the inner boundary, we prescribe 100 eV for the temperatures and 10^{13} cm^{-3} for the density. As expected, the electron temperature reflects the structure of the magnetic field better than the ion temperature and much better than the density because of the differences in the parallel transport (see figure 6). Indeed, the electron temperature in the island is almost constant, the ion temperature has a noticeable gradient across the island and the density demonstrates an even stronger gradient. The statistical noise in the density profile is stronger than in either temperature, because their larger parallel transport works like a smoothing filter. The same behaviour can be seen for all sections of the device.

11. Outlook and summary

An interesting collaboration is planned with the DIII-D team. In this device a special set of compensation coils (so-called C-coils) is used to optimize the core plasma performance by nulling a presumed error field at the $q = 2$ surface. As a

consequence, in some operational scenarios an ergodic region arises at the edge, as can be seen from field line tracing calculations [15]. E3D will be used to investigate the effect of stochasticity on the transport properties and by this on the plasma distribution. Even without active C-coils (due to coil misalignments), the separatrix is replaced by a thin ergodic layer, whose impact on the plasma is also interesting in its own right.

We demonstrated that proper modelling of plasma transport in ergodic magnetic fields requires the use of local magnetic coordinates. The price we have to pay is the inclusion of the full metric tensor in the numerics. By doing this, all transport terms can be treated consistently without any approximation. This method has a large variety of applications, some of which have been presented here.

References

[1] Runov A.M., Reiter D., Kasilov S.V., Kernbichler W. and Heyn M.F. 2001 *Phys. Plasmas* **8** 916–30

[2] Runov A., Kasilov S., Riemannn J., Borchardt M., Reiter D. and Schneider R. 2002 *Contrib. Plasma Phys.* **42** 169–74

[3] Kasilov S.V., Reiter D., Runov A.M., Kernbichler W. and Heyn M. 2002 *Plasma Phys. Control. Fusion* **44** 985–1004

[4] Runov A., Kasilov S., Reiter D., McTaggart N., Bonnin X. and Schneider R. 2003 *J. Nucl. Mater.* **313–316** 1292–7

[5] Abdullaev S.S., Finken K.H., Jakubowski M.W., Kasilov S.V., Kobayashi M., Reiser D., Reiter D., Runov A. and Wolf R. 2003 *Nucl. Fusion* **43** 299–313

[6] Runov A., Kasilov S., Schneider R. and Reiter D. 2004 *Contrib. Plasma Phys.* **44** 18–24

[7] Finken K.H. *et al* 1997 Dynamic ergodic divertor *Fusion Eng. Des.* **37** 1 (special issue)

[8] Rechester A.B. and Rosenbluth M.N. 1978 *Phys. Rev. Lett.* **40** 38–41

[9] D'Haeseleer W.D., Hitchon W.N.G., Callen J.D. and Shohet J.L. 1991 *Flux Coordinates and Magnetic Field Structure* (Berlin: Springer)

[10] Kloeden P.E. and Platen E. 1999 *Numerical Solution of Stochastic Differential Equations* 3rd edn (New York: Springer)

[11] Milstein G.N. 1978 *Theory Probab. Appl.* **23** 396–401

[12] Tongue B.H. 1987 *Physica* D **8** 401–8

[13] Montvai A. and Düchs D.F. 1993 *Physics Computing '92, (Prague, 1992)* (Singapore: World Scientific) p 417

[14] Hogeweij G.M.D. *et al* 1998 *Nucl. Fusion* **38** 1881–91

[15] Evans T.E. *et al* 2002 *Phys. Plasmas* **9** 4957–67